Calibration of rototilled soil block discrete element parameters after rotary tillage in rape planting by machinery

Fanggang Shi[1], Mingliang Wu[1,2], Zhihao Zhao[1], Haiyang Chen[1], Xiaohu Jiang[1], Wei Quan[3*]

(1. *College of Mechanical and Electrical Engineering, Hunan Agriculture University, Changsha 410128, China*;
2. *Hunan Provincial Engineering Technology Research Center for Modern Agricultural Equipment, Changsha 410128, China*;
3. *College of Orient Science & Technology, Hunan Agricultural University, Changsha 410128, China*)

Abstract: This study sought to construct and empirically validate a discrete element method (DEM) particle model representing post-tillage soil blocks. This model was developed to facilitate a detailed examination of granular movement and contact mechanics during the shaping process of planting chambers for rape plants. The research specifically targeted the sticky, cohesive soil prevalent in rice paddy fields of the middle and lower Yangtze River region. Simulations were conducted using EDEM software to improve the accuracy with which soil-tool interactions are predicted for the design and optimization of mechanical transplanters. The physical and bonding parameters of the sticky soil were calibrated using the Hertz-Mindlin with Johnson-Kendall-Roberts (JKR) contact model and Hertz-Mindlin with Bonding contact model. A particle replacement method was adopted to create a discrete element model of cohesive soil aggregates with different shapes and sizes after rotary tillage. The accumulation angle of soil aggregates was used as the evaluation index in both the simulation and physical experiments. Design-Expert software was used to design a four-factor, three-level simulation experiment to identify the optimal parameter combinations for the physical and mechanical properties of the sticky soil and the JKR contact model, which comprised a soil-soil static friction coefficient of 0.32, soil-soil rolling friction coefficient of 0.10, soil-steel static friction coefficient of 0.51, and surface energy of soil for the JKR model of 5.50 J/m^2. Next, the steepest climbing test and Box-Behnken orthogonal combination test were then used to narrow down the range of values for the significant factors and identify the optimal parameter combinations for the bonding contact model parameters, which included a bonding bond normal contact stiffness of 2.1×10^6 N/m, a bonding bond tangential contact stiffness of 2.2×10^6 N/m, a normal ultimate stress of 0.55 MPa, a tangential ultimate stress of 0.55 MPa, and a bonding radius of 12 mm. Field experiments were conducted using a flat box device to measure the soil evenness and firmness after ridge formation and compaction by a rotary tiller. The results of these experiments were compared with the discrete element simulation optimization results. The relative errors between the field test results and the simulation test results for soil flatness and compaction were 10.7% and 9.8%, respectively, which indicated good accuracy of the parameters calibrated and optimized by EDEM discrete element simulation software. Overall, this research can provide a reference for understanding the working mechanism and optimizing the parameters of soil touching components in rape transplanting equipment.

Keywords: rape, soil block, soil firmness, discrete element method, parameter calibration
DOI: 10.25165/j.ijabe.20261902.9590

Citation: Shi F G, Wu M L, Zhao Z H, Chen H Y, Jiang X H, Quan W. Calibration of rototilled soil block discrete element parameters after rotary tillage in rape planting by machinery. Int J Agric & Biol Eng, 2026; 19(2): 28–38.

1 Introduction

Rotary tillage operation is one of the important tillage processes used before mechanized planting of oilseed rape in the middle and lower reaches of the Yangtze River[1]. After rotary tillage, the soil forms aggregates of various sizes. Establishing an accurate discrete element simulation model of this post-tillage soil not only improves the accuracy of simulating the operation process of the soil-touching components but also provides a basis for studying the interaction mechanism between these components and the soil, as well as for optimizing their parameters.

Parameter calibration is crucial for ensuring the accuracy of discrete element models for bulk materials like soil. The accuracy is highly dependent on factors such as particle size and shape, calibration methods, and contact model parameters[2-4]. Over the past decade, various approaches have been adopted for constructing discrete element models. In this respect, contact models have been developed for spherical particles in sandy loam soil by combining a linear adhesion model with a delayed elasticity model[5,6]. This approach effectively represents both the physical properties of soil particles and the plastic deformation that occurs under external forces. Ucgul et al.[7] constructed a discrete element model to analyze plow-soil interaction. Their work explored the changing patterns of soil disturbance, tillage resistance, and plow furrow profile quality. Besides, Ding et al.[8] developed a discrete element model specifically for deep loosening tillage of clayey rice soils. Their model utilized the Hertz-Mindlin with Bonding model, which incorporates bonding forces between spherical particles, making it

Received date: 2024-12-05 **Accepted date:** 2025-11-21
Biographies: Fanggang Shi, PhD, research interest: innovative design of agricultural machinery, Email: shifanggang@stu.hunau.edu.cn; **Mingliang Wu,** Professor, research interest: innovative design of agricultural machinery, Email: mlwu@hunau.edu.cn; **Zhihao Zhao**, PhD, research interest: innovative design of agricultural machinery, Email: xiaozhaooo@stu.hunau.edu.cn; **Haiyang Chen**, PhD, research interest: innovative design of agricultural machinery, Email: leo620821@126.com; **Xiaohu Jiang**, Associate Professor, research interest: agricultural machinery, Email: xiaohujiang@hunau.edu.cn.
***Corresponding author: Wei Quan**, Associate Professor, research interest: innovative design of agricultural machinery. College of Orient Science & Technology, Hunan Agricultural University, Changsha 410128, China. Tel: +86-15874187102, Email: B20170022@126.com.

suitable for soils with high inter-particle bonding. While numerous studies have focused on building discrete element models using individual spherical particles[9-12], it is now understood that most soil components encountered in real-world operations have irregular, polyhedral shapes. Indeed, the shape and size of these particles significantly impact the accuracy of simulation calibration[13]. Zhang et al.[14] investigated the effects of particle size, mass, and calibration methods on the stacking angle of simulated soil. Their findings demonstrated that particle shape and morphology exerted a relatively large impact on the inter-particle static friction coefficient and that combined particles yielded a lower relative error compared to spherical particles. Wang et al.[15] established a discrete element model for a complex seedling substrate composed of a mixture of particle types. They employed a Box-Behnken test for parametric calibration of the model parameters and achieved consistency between measured and simulated values. Other studies[13,16] have utilized a 3D scanning inverse modeling technique with a particle filling method to construct soil blocks with varying particle sizes, followed by calibration of the parameters governing the interactions between these particles. In earlier research[17,18], the displacement of soil particles of different sizes during tillage was modeled, analyzing the macroscopic and microscopic movements of soil at various locations. In summary, existing research has primarily focused on building discrete element models of soil using individual spherical particles or combined particles, often for soils with smaller particle sizes. However, there has been a paucity of studies on large-grained soil blocks formed after rotary tillage, particularly regarding discrete element simulation models that consider the mechanical properties between the combined particles within these aggregates[19,20].

Therefore, this study focused on clay-rich soil blocks formed after rotary tillage in the southern rice-fallow rotation area. In actual tillage operations, the issue arises where insufficient soil crumb size after rotary tillage leads to significant unevenness in the soil surface, affecting crop planting. Furthermore, though research on larger soil clods remains limited, a discrete element model of these clayey soil blocks was established using the Hertz-Mindlin with JKR and the Hertz-Mindlin with Bonding contact models. This approach combined physical and simulation tests, with the stacking angle and firmness of the soil blocks serving as response values. The physical parameters and bonding parameters of the soil blocks contact model were determined through a combination of tests: the central composite design, the Plackett-Burman test, the steepest ascent test, and the Box-Behnken test. Using the optimized parameters, a discrete element model of soil troughs composed of soil blocks with varying grain sizes was established. Finally, the accuracy of the model was validated by comparing field measurements of compartment flatness and firmness with the simulation results.

2 Measurement of soil characterization parameters

2.1 Test materials and equipment

This study focused on clay-rich soil blocks formed after rotary tillage. Samples were collected from a field plot (28°34′21″N, 113°42′96″E) belonging to the Liuyang City Yingchang Agricultural Machinery Professional Cooperative. The samples were taken from the top 20 cm (0-200 mm) of soil tilled by a rotary tiller in the fall, following rice harvest. The following instruments and equipment were used: a DF604-15 tractor, a rotary tiller, a stacking angle measuring device, a JK-750-I soil firmness tester, an LC-DHS-10A moisture rapid analyzer, a ring cutter, a soil scraper, electronic scales, a tape measure, an aluminum box, and a steel ruler.

2.2 Test methods

Sampling measurements were performed using the diagonal five-point method at randomly selected and independent locations within the sampling area. The particle size distribution of the soil blocks collected from the sampling area was then determined.

2.2.1 Determination of soil density and moisture content

The ring knife method was used to determine soil density. Five sampling locations were chosen using the diagonal five-point method. The ring knife (inner diameter 50.46 mm, height 50.00 mm, volume 100 cm^3) was gently pressed into the soil until there was no gap. The soil around the ring knife was then cleaned, and the excess soil at both ends was scraped off to create a flat surface. Finally, the ring knife was carefully removed. The average moisture content of the soil, measured using a rapid moisture analyzer (accuracy 0.01%), was 25.60%. The average density, determined using an electronic scale (precision 0.01 g), was 2680 kg/m^3.

2.2.2 Soil blocks particle size statistics

The test field of 10 m×30 m area was tilled using a rotary tiller manufactured by Hunan Sanglaite Agricultural Machinery Company. The tiller was equipped with T245 rotary knives in a helical arrangement. It operated at a speed of 240 r/min and a forward speed of 1.68 km/h. Following rotary tillage, the five-point sampling method was used to collect soil samples from a depth of 0 to 200 mm (Figure 1). Each sample point covered an area of 500 mm×500 mm×200 mm (0.05 m^3). During sampling, the particle size distribution and volume fraction of soil pieces were determined based on the longest side of the sample area, as listed in Table 1.

Figure 1 Soil blocks after rotary tillage

Table 1 Size classification and volume fraction of soil

Soil block size/mm	10-29	30-69	70-109	110-150	≤10
Quantities	143	57	29	7	3079
Volume fraction/%	2.4	14.9	44.0	32.2	6.5

2.2.3 Physical test of soil blocks stacking angle

The stacking angle of the soil blocks was measured using the box draw plate method[13,21]. The measuring device, constructed from steel (Figure 2), consisted of three parts: a box (400 mm×350 mm×400 mm), a baffle plate (440 mm×400 mm), and a base plate (1000 mm×1200 mm). To promote the homogeneous distribution of the soil blocks during stacking and create an unconfined pile on the horizontal base plate, the baffle plate was slowly withdrawn upwards. Once the soil blocks had naturally settled and reached a stable state, the angle between the inclined plane formed by the pile and the horizontal base plate was considered the soil blocks stacking angle. A high-definition camera positioned on the right side of the device captured an image of the stabilized pile. The stacking angle was then determined using the least squares method by fitting a straight line to the boundary curve of the pile.

The image processing method involved using Photoshop software to convert the image to grayscale, effectively capturing the soil blocks pile’s outer edge contour. Then, Matlab software was used to read the positions of points along this contour and fit a straight line to them, as shown in Figure 3. With the lower left corner of the measuring device designated as the coordinate origin, the x-axis extended to the right along the device’s lower edge, and the y-axis extended upwards from the lower left corner. The soil blocks stacking angle was calculated using the inverse tangent value of the fitted straight line’s slope. The test was repeated four times, and the average slope of the fitted lines was 0.81. This corresponded to an average stacking angle of 39.0° for the physical soil blocks test.

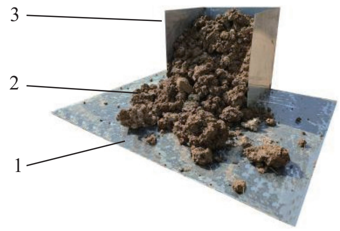

1. Base plate 2. Soil blocks 3. Box

Figure 2 Stacking angle measurement device

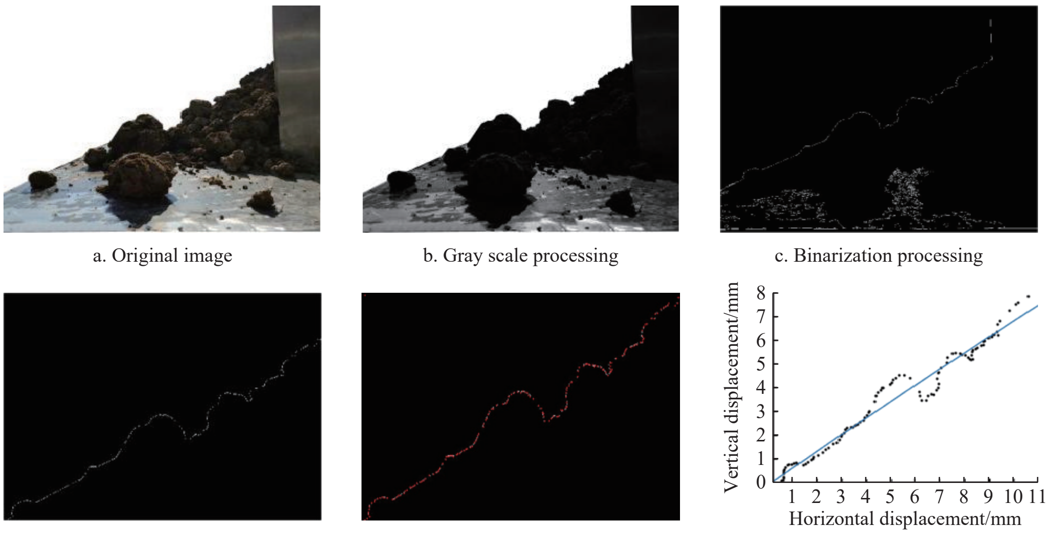

a. Original image b. Gray scale processing c. Binarization processing

d. Cutting boundary curves e. Scatter sampling f. Straight line fitting

Figure 3 Image analysis by Matlab for stacking angle

2.2.4 Soil firmness measurement test

Soil samples used for both the firmness measurement and the stacking angle test were collected from the same field. A digital JK-750-I soil firmness tester was used to determine soil firmness. To perform the test, the soil blocks were first placed horizontally. Then, the cone tip of the soil firmness tester was slowly inserted into the soil blocks, and the reading on the instrument was recorded (Figure 4). The firmness of three different-sized soil blocks was measured at different insertion depths. The test was repeated four times to obtain an average value. As listed in Table 2, the results revealed minimal variation in the firmness of different-sized soil blocks at the same depth. Therefore, the firmness of the soil blocks measured at a penetration depth of 30 mm was chosen as the response value for simulation calibration. The average value for this measurement was 201.6 kPa.

Figure 4 Soil block firmness detection test

Table 2 Soil block firmness

Depth/mm	Firmness of soil blocks with different particle sizes/kPa			Average
	50 mm	90 mm	130 mm	
5	91.1	90.2	92.0	91.1
10	133.5	120.3	131.7	128.5
20	181.3	170.6	182.1	178.0
30	202.9	195.4	206.5	201.6
50	0	274.1	293.6	283.9

3 Simulated calibration of soil contact parameters

3.1 Selection of contact model

Due to the mutual attraction between soil blocks, the Hertz-Mindlin with JKR contact model was selected to represent the interactions between them. Besides, to account for the bonding forces within the soil aggregates, the Hertz-Mindlin with bonding contact model was chosen to describe the interactions between particles inside the aggregates. This consideration incorporates the potential crushing of soil blocks and particle fracture under external forces[22,23]. The parameters of both models were then calibrated accordingly.

3.2 Simulation parameters

Drawing on the results of the previous tests and the parameter selection ranges reported in the literature[9,14,24,25], the range of physical parameters for the soil-steel contact was established. For the interactions between particles within the soil blocks, the bonding strength was primarily determined by the bonding parameters, which include normal contact stiffness, tangential contact stiffness, normal ultimate stress, tangential ultimate stress, and bonding radius. Considering existing research and studies on the discrete element parameter modeling of similar materials[26-29], the preliminary discrete element simulation parameter range for the soil blocks is presented in Table 3.

Table 3 Parameters and level required in EDEM simulation

Parameters	Level			Literature sources
	–1	0	1	
Soil-soil recovery coefficient	0.45			[9,13,25]
Soil-soil static friction coefficient	0.3	0.6	0.9	
Soil-soil rolling friction coefficient	0.05	0.10	0.15	
Soil-steel recovery coefficient	0.4			[9,25]
Soil-steel static friction coefficient	0.4	0.5	0.6	
Soil-steel rolling friction coefficient	0.15			[9,25]
Soil JKR surface energy/$J\cdot m^{-2}$	3	6	9	
Soil-soil normal contact stiffness/$N\cdot m^{-1}$	1.0×10^6	4.0×10^6	7.0×10^6	
Soil-soil tangential contact stiffness/$N\cdot m^{-1}$	1.0×10^6	4.0×10^6	7.0×10^6	
Soil-soil normal ultimate stress/MPa	0.10	0.55	1.0	
Soil-soil tangential ultimate stress/MPa	0.10	0.55	1.0	
Bond radius/mm	11	13	15	

3.3 Simulation calibration test of the stacking angle of the clay soil blocks

3.3.1 Simulation modeling

The particle size distribution and size of the soil blocks were determined through physical tests. To ensure the virtual soil tank closely resembled the actual tank while facilitating efficient modeling and calculations, the soil blocks' shape was simplified to a sphere. Soil blocks with larger particle size fractions were generated based on the statistically determined volume fractions. Three aggregate sizes with median diameters of 50 mm, 90 mm, and 130 mm were chosen for modeling the soil blocks. The smallest spherical particles were set to a diameter of 10 mm[30]. Within the software, the Hertz-Mindlin with JKR model was used for the stacking angle simulation test. The soil blocks were approximated as a sphere, and a rigid model of the soil blocks with particle sizes of 50 mm, 90 mm, and 130 mm was constructed sequentially by substituting small spherical particles using the particle substitution method (Figure 5).

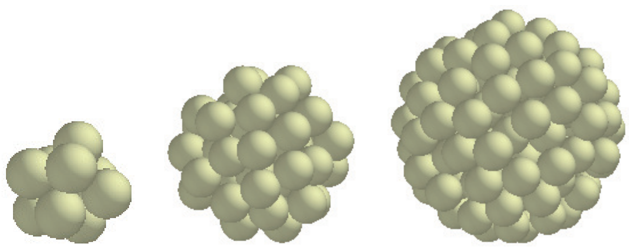

a. 50 mm diameter soil blocks   b. 90 mm diameter soil blocks   c. 130 mm diameter soil blocks

Figure 5 Soil blocks penetration resistance detection test

To ensure the accuracy of the simulation analysis, a three-dimensional model of the box baffle plate device was created in a 1:1 scale and saved in .stl format for import into EDEM software. The baffle plate speed was set to a uniform linear motion of 0.05 m/s in the upward direction. The particles were allowed to move under the influence of gravity until they reached a stable, stationary pile. The stacking angle of the pile was then measured, signifying the completion of the simulation. During the simulation test, EDEM post-processing generated a side-view image of the pile. The stacking angle determination direction was consistent with the method described previously (Figure 6). The material property for the plate was set to steel. The intrinsic parameters used for the soil and steel in the simulation tests, adapted from the literature[5,27], are presented in Table 4.

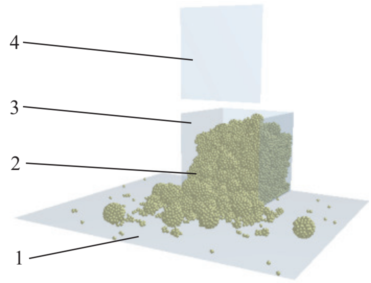

1. Base plate 2. Soil blocks 3. Box 4. Baffle plate

Figure 6 Stacking angle measurement device

Table 4 Intrinsic parameters of soil and steel

Parameters	Value
Soil density ρ/$kg\cdot m^{-3}$	2680
Poisson's ratio for soil v_1	0.38
Soil shear modulus G_1/MPa	1.2
Poisson's ratio of steel v_2	0.3
Steel shear modulus G_3/MPa	7.0×10^4
Steel density ρ/$kg\cdot m^{-3}$	7850

3.3.2 Centralized combined experimental design

Parameters X_1 (soil-soil static friction coefficient), X_2 (soil-soil rolling friction coefficient), X_3 (soil-steel static friction coefficient), and X_4 (soil JKR surface energy) were chosen for optimization. A four-factor, five-level simulation test was conducted using the central composite design method, with the soil stacking angle as the response variable. The design of the simulation test is listed in Table 5.

Design-Expert software was used to develop a second-order regression model for the soil blocks stacking angle (θ) using four independent variables (coded values). The model equation is a quadratic polynomial:

$$\theta = 44.17 + 4.08X_1 + 2.08X_2 + 0.42X_3 + 0.25X_4 + 2.13X_1X_2 - 1.25X_1X_3 - 0.88X_1X_4 + 0.50X_2X_3 + 0.13X_2X_4 - 0.50X_3X_4 - 1.50X_1^2 - 0.25X_2^2 + 0.63X_3^2 + 1.50X_4^2 \quad (1)$$

An analysis of variance (ANOVA) was performed on the experimental model (Table 5). As listed in Table 6, a high statistical significance was obtained (P-value=0.0045), indicating a strong relationship between the stacking angle (dependent variable) and all independent variables. The coefficient of determination (R^2=0.7970) was close to 1, suggesting a good fit and high reliability of the model equations. Besides, the coefficient of variation (CV=8.13%) and adequate precision (9.3029) indicated good model reliability and accuracy.

As listed in Table 6, the simulated linear term X_1 (soil-soil static friction coefficient) exerted a highly significant effect on the stacking angle. The linear term X_2 (soil-soil rolling friction coefficient), interaction term X_1X_2, and quadratic terms X_1^2 and X_4^2 also exhibited significant effects. Analyzing individual factors, the order of their influence on the stacking angle was: X_1 (soil-soil static friction coefficient) > X_2 (soil-soil rolling friction coefficient) > X_3 (soil-steel static friction coefficient) > X_4 (soil JKR surface energy).

Table 5 Design and results of soil block accumulation simulation test

Set	Factors				Stacking angle/(°)
	X_1	X_2	X_3	X_4	
1	0.3	0.05	0.4	3	41
2	0.9	0.05	0.4	3	47
3	0.3	0.15	0.4	3	43
4	0.9	0.15	0.4	3	53
5	0.3	0.05	0.6	3	42
6	0.9	0.05	0.6	3	48
7	0.3	0.15	0.6	3	45
8	0.9	0.15	0.6	3	56
9	0.3	0.05	0.4	9	41
10	0.9	0.05	0.4	9	45
11	0.3	0.15	0.4	9	39
12	0.9	0.15	0.4	9	55
13	0.3	0.05	0.6	9	45
14	0.9	0.05	0.6	9	38
15	0.3	0.15	0.6	9	45
16	0.9	0.15	0.6	9	51
17	0	0.10	0.5	6	25
18	1.2	0.10	0.5	6	48
19	0.6	0	0.5	6	41
20	0.6	0.20	0.5	6	46
21	0.6	0.10	0.3	6	44
22	0.6	0.10	0.7	6	46
23	0.6	0.10	0.5	0	43
24	0.6	0.10	0.5	12	54
25	0.6	0.10	0.5	6	43
26	0.6	0.10	0.5	6	44
27	0.6	0.10	0.5	6	45
28	0.6	0.10	0.5	6	44
29	0.6	0.10	0.5	6	44
30	0.6	0.10	0.5	6	45

Table 6 ANOVA of quadratic polynomial model of central composite design test

Source of variance	Sum of squares	Freedom	Mean square	F-value	p-value
Model	783.80	14	55.99	4.21	0.0045**
X_1	400.17	1	400.17	30.06	<0.0001**
X_2	104.17	1	104.17	7.83	0.0135*
X_3	4.17	1	4.17	0.3130	0.5841
X_4	1.50	1	1.50	0.1127	0.7418
X_1X_2	72.25	1	72.25	5.43	0.0342*
X_1X_3	25.00	1	25.00	1.88	0.1907
X_1X_4	12.25	1	12.25	0.9203	0.3526
X_2X_3	4.00	1	4.00	0.3005	0.5916
X_2X_4	0.2500	1	0.2500	0.0188	0.8928
X_3X_4	4.00	1	4.00	0.3005	0.5916
X_1^2	61.71	1	61.71	4.64	0.0480*
X_2^2	1.71	1	1.71	0.1288	0.7247
X_3^2	10.71	1	10.71	0.8049	0.3838
X_4^2	61.71	1	61.71	4.64	0.0480*
Residuals	199.67	15	13.31		
Lack of fit	196.83	10	19.68	34.74	0.0005**
Error	2.83	5	0.5667		
Total sum	983.47	29			

Note: p indicates the probability level criterion to test whether it is significant; p<0.05 denotes that the model term is significant, expressed by "*"; p<0.01 indicates that the model term is highly significant, "**"; p>0.1 indicates that the model term is not significant.

To match the experimentally measured soil blocks stacking angle of 39.0°, the fitted equations were solved numerically. This optimization process yielded the following optimal values for the soil parameters: soil-soil static friction coefficient (0.32), soil-soil rolling friction coefficient (0.10), soil-steel static friction coefficient (0.51), and soil JKR surface energy (5.50 J/m^2).

3.3.3 Validation of optimal parameters for soil blocks stacking angle

To validate the calibrated soil contact parameters, a soil block stacking simulation test was conducted using these values. The calibrated stacking angle (41.0°) exhibited a 5.1% difference compared to the measured value (39.0°). This result indicated that the stacking angle-based calibration of the soil-steel and soil-block contact parameters achieved good accuracy and reliability.

3.4 Soil firmness simulation calibration test

The Hertz-Mindlin with Bonding contact model considers normal contact stiffness, tangential contact stiffness, normal ultimate stress, and tangential ultimate stress. These parameters were related to the amount of overlap between particles and are dynamically calculated based on the contact process. They exhibited a positive correlation with the simulation time step size and cannot be directly measured, necessitating calibration and optimization.

To achieve this, Design-Expert software was first used to perform a Plackett-Burman screening design. This identified the physical parameters with significant effects on the firmness of the soil blocks during the physical test. Subsequently, the steepest climb test further narrowed down the parameter range of these significant factors. Finally, a Box-Behnken design was employed for regression analysis and parameter optimization of the simulation model. This process determined the optimal parameters for the discrete element simulation using the Hertz-Mindlin with Bonding model.

3.4.1 Soil blocks modeling

A single soil block was modeled using the Hertz-Mindlin with Bonding contact model. This approach simulated the soil blocks as a flexible assembly of bonded particles, allowing them to be crushed under external forces. The crushing process of the soil blocks can, therefore, be realistically captured in the simulation. A 3D model of the soil blocks in .stl format, exported from Pro/E 5.0 software, was imported into EDEM software as the geometry. At the upper end of the container, a particle plant was defined to generate spherical particles with a certain initial velocity. To promote better packing and mobility, these particles were assigned a lower coefficient of restitution (collision recovery coefficient) and appropriate kinetic and static friction coefficients. Besides, a higher gravitational acceleration was set to achieve denser packing within the voids. Once the spherical particles filled the model, the center coordinates of all particles were exported from the EDEM post-processing interface in a .csv data file. The particle replacement method was then used to generate agglomerates formed by bonding multiple small spherical particles. The replacement particles were assigned a larger bonding force to establish inter-particle bonding. The particle contact radius was set to 1.2 times the diameter of the small spherical particles (12 mm). The bonding radius, a parameter to be calibrated, defines the effective zone of inter-particle bonding. These steps completed the creation of the single-soil blocks simulation model, as illustrated in Figure 7.

3.4.2 Simulation modeling for soil blocks firmness measurement

Drawing on the calibrated soil blocks parameters, a soil blocks model was created within EDEM software. A separate 3D model of a conical steel needle (radius 6 mm) was established in a 1:1 scale.

The steel needle was assigned a material of steel, with physical properties identical to those previously defined. This model was then imported into EDEM software for simulation experiments. The falling speed of the steel needle was set to 0.01 m/s, and the falling duration was set to 3 s. The simulation setup is illustrated in Figure 8.

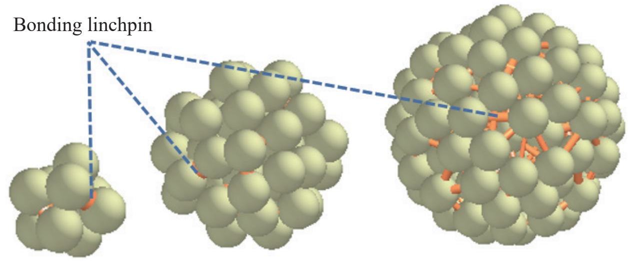

a. 50 mm diameter soil blocks b. 90 mm diameter soil blocks c. 130 mm diameter soil blocks

Figure 7 Soil blocks obtained by particle replacement

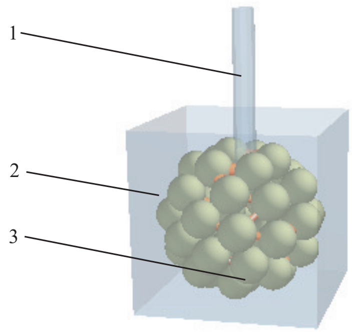

1. Conical steel needle 2. Particle factory 3. Soil blocks

Figure 8 Firmness measurement simulation modeling

Soil firmness P is calculated as:

$$P = \frac{F}{S} \tag{2}$$

where, F denotes the maximum force applied to the conical steel needle, N; S represents the cross-sectional area of the conical steel needle in contact with the soil mass, m^2.

3.4.3 Plackett-Burman screening test and significance analysis

The Plackett-Burman design employs 12 test sets to evaluate 11 factors. Five of these factors are actual parameters: X_5 (bond normal contact stiffness), X_6 (bond tangential contact stiffness), X_7 (normal ultimate stress), X_8 (tangential ultimate stress), and X_9 (bond radius). Each actual parameter is tested at two levels, denoted by the codes +1 (high) and –1 (low). Six virtual blank columns (X_{10} to X_{15}) are also included in the design. The experimental design and results are presented in Table 7.

As listed in Table 8, the firmness exhibited significant fluctuations across different factor levels. The data from Table 7 was analyzed using ANOVA in Design-Expert software. The resulting model was statistically significant, and the factors influencing firmness were ranked in descending order of significance as X_5, X_6, X_9, X_8, X_7. The p-values of X_5, X_6, and X_9 were less than 0.05, indicating a significant effect on the response values (firmness). In contrast, the p-values of X_8 and X_7 were greater than 0.05, suggesting a negligible impact on the response. Consequently, X_5, X_6, and X_9 were chosen for further investigation using the steepest climb test and Box-Behnken test.

3.4.4 Steepest climb test

Following the Plackett-Burman screening, a steepest climb test was conducted to refine the range of significant parameters (X_5, X_6, and X_9) identified for firmness. This optimization technique aimed to rapidly identify the region containing the optimal values for these parameters. During the steepest climb tests, intermediate-level values were assigned to the non-significant parameters (X_7 and X_8) that had minimal influence on firmness. These non-significant parameters were fixed at 0.55 MPa for both normal ultimate stress (X_7) and tangential ultimate stress (X_8). The design and results of the steepest climb test are presented in Table 9.

Table 7 Results of the Plackett-Burman design (P-BD) test

Set	Factors											Firmness/kPa
	X_5	X_6	X_7	X_8	X_9	X_{10}	X_{11}	X_{12}	X_{13}	X_{14}	X_{15}	
1	1	1	–1	1	1	1	–1	–1	–1	1	–1	582.7
2	–1	1	1	–1	1	1	1	–1	–1	–1	1	380.2
3	1	–1	1	1	–1	1	1	1	–1	–1	–1	283.2
4	–1	1	–1	1	1	–1	1	1	1	–1	–1	380.2
5	–1	–1	1	–1	1	1	–1	1	1	1	–1	179.5
6	–1	–1	–1	1	–1	1	1	–1	1	1	1	118.0
7	1	–1	–1	–1	1	–1	1	1	–1	1	1	381.1
8	1	1	–1	–1	–1	1	–1	1	1	–1	1	440.3
9	1	1	1	–1	–1	–1	1	–1	1	1	–1	204.3
10	–1	1	1	1	–1	–1	–1	1	–1	1	1	274.1
11	1	–1	1	1	1	–1	–1	–1	1	–1	1	381.1
12	–1	–1	–1	–1	–1	–1	–1	–1	–1	–1	–1	118.0

Table 8 Analysis of Plackett-Burman design test results

Factors	Sum of squares	Freedom	Mean square	F-value	p-value
Model	186 400.0	5	37 272.82	7.74	0.0135*
X_5	56 402.94	1	56 402.94	11.72	0.0141*
X_6	53 453.40	1	53 453.40	11.10	0.0158*
X_7	8421.70	1	8421.70	1.75	0.2341
X_8	8316.07	1	8316.07	1.73	0.2367
X_9	59 769.97	1	59 769.97	12.42	0.0125*
Residuals	28 882.98	6	4813.83		
Total sum	215 200.0	11			

Table 9 Steepest climb test design and results

Set	X_5/N·m^{-1}	X_6/N·m^{-1}	X_9/mm	Firmness/kPa	Error/%
1	1.0×10^6	1.0×10^6	11	118.0	–41.5
2	2.5×10^6	2.5×10^6	12	197.6	–2.0
3	4.0×10^6	4.0×10^6	13	397.0	96.9
4	5.5×10^6	5.5×10^6	14	492.5	144.3
5	7.0×10^6	7.0×10^6	15	582.7	189.0

The steepest climb test results for soil block firmness at a penetration depth of 30 mm are inconclusive regarding the optimal values for parameters X_5, X_6, and X_9. While the test covered a range between the low and high firmness levels (levels No. 1 and No. 3) by adjusting these parameters, it did not pinpoint the specific combination that achieves the target firmness of 201.6 kPa. Therefore, to determine the optimal parameter combination for the desired firmness, a Box-Behnken test and subsequent regression modeling analysis were employed. This approach focuses on the identified significant factors (X_5, X_6, and X_9).

3.4.5 Box-Behnken tests and regression models

Leveraging the insights from the steepest climb test, a Box-Behnken test was designed to optimize the firmness of the soil blocks at a penetration depth of 30 mm. The design scheme and results of the Box-Behnken test are presented in Table 10.

Table 10 Box-Behnken experimental design and results

Set	Factors			Firmness/ kPa
	X_5/N·m^{-1}	X_6/N·m^{-1}	X_9/mm	
1	1.0×10^6	1.0×10^6	12	133.5
2	4.0×10^6	1.0×10^6	12	253.8
3	1.0×10^6	4.0×10^6	12	236.1
4	4.0×10^6	4.0×10^6	12	359.9
5	1.0×10^6	2.5×10^6	11	171.8
6	4.0×10^6	2.5×10^6	11	285.6
7	1.0×10^6	2.5×10^6	13	213.1
8	4.0×10^6	2.5×10^6	13	345.7
9	2.5×10^6	1.0×10^6	11	159.1
10	2.5×10^6	4.0×10^6	11	244.9
11	2.5×10^6	1.0×10^6	13	193.6
12	2.5×10^6	4.0×10^6	13	357.2
13	2.5×10^6	2.5×10^6	12	229.0
14	2.5×10^6	2.5×10^6	12	229.0
15	2.5×10^6	2.5×10^6	12	229.0
16	2.5×10^6	2.5×10^6	12	229.0
17	2.5×10^6	2.5×10^6	12	229.0

The experimental results were used to develop a second-order regression model for soil blocks firmness (Y) using Design-Expert software. The model incorporates three independent variables (coded values) and is expressed by a quadratic polynomial equation:

$$Y = 229.0 + 61.31X_5 + 57.26X_6 + 31.02X_9 + 0.88X_5X_6 + 4.70X_5X_9 + 19.45X_6X_9 + 16.09X_5^2 + 0.74X_6^2 + 8.96X_9^2 \quad (3)$$

An ANOVA was performed on the experimental model (Table 10). The results, presented in Table 11, indicated a highly statistically significant model (p<0.0001), suggesting a robust relationship between the dependent variable (firmness) and all the independent variables. The coefficient of determination (R^2= 0.9931) and the adjusted coefficient of determination (R^2_{adj}=0.9843) were both very close to 1, indicating the model's high reliability and exceptional goodness-of-fit. Besides, the coefficient of variation (CV=3.38%) and adequate precision (37.9226) indicated superior model confidence and accuracy.

As listed in Table 11, the linear terms (X_5, X_6, and X_9), the interaction term (X_6X_9), and the quadratic term (X_5^2) of the simulation all yielded highly significant effects on firmness. Analyzing the individual factors, each one exhibits a highly significant impact on firmness. When considering interactions, the order of their influence on firmness is X_6X_9>X_5X_9>X_5X_6.

Table 11 ANOVA of the quadratic polynomial model of test

Source of variance	Sum of squares	DoF	Mean square	F-value	p-value
Model	67 125.95	9	7458.44	112.19	<0.0001**
X_5	30 073.78	1	30 073.78	452.37	<0.0001**
X_6	26 231.95	1	26 231.95	394.58	<0.0001**
X_9	7700.40	1	7700.40	115.83	<0.0001**
X_5X_6	3.06	1	3.06	0.0461	0.8362
X_5X_9	88.36	1	88.36	1.33	0.2868
X_6X_9	1513.21	1	1513.21	22.76	0.0020**
X_5^2	1089.72	1	1089.72	16.39	0.0049**
X_6^2	2.29	1	2.29	0.0344	0.8580
X_9^2	338.22	1	338.22	5.09	0.0587
Residuals	465.37	7	66.48		
Lack of fit	465.37	3	155.12		
Error	0.0	4	0.0		
Total sum	67 125.95	16			

3.4.6 Regression model interaction effects analysis

This experiment investigated the firmness of soil blocks (penetration depth: 30 mm) as an evaluation index for calibrating soil simulation model parameters. Design-Expert software was used to fit a quadratic multiple regression model to the data. The resulting response surfaces and contour plots in Figure 9 illustrate the interactions between parameters affecting the objective function (firmness). These interactions were further analyzed, focusing on the normal contact stiffness and tangential contact stiffness of the bond (Figure 9a), the tangential contact stiffness and the bond radius of the bond (Figure 9b), and the normal contact stiffness and bond radius (Figure 9c). The steeper slopes of the response surface in Figures 9 indicated that these three interaction terms yielded more significant effects on firmness. When one factor was fixed, firmness generally increased as the other two factors increased. This conclusion aligned with the findings from the ANOVA results.

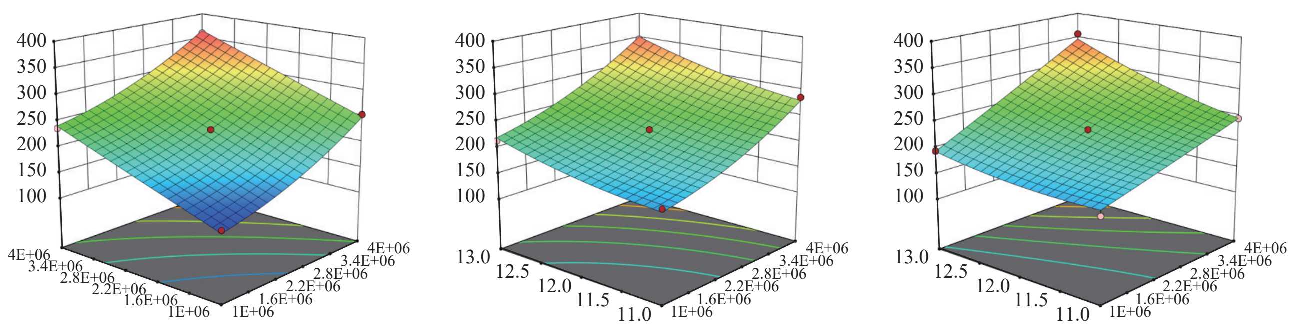

a. Interaction between X_5 and X_6 b. Interaction between X_5 and X_9 c. Interaction between X_6 and X_9

Figure 9 Effect of interaction on firmness

3.4.7 Validation of optimal parameter model for soil firmness

The regression equation was then employed in Design-Expert software to optimize the model and achieve the target firmness of 201.6 kPa. This optimization process yielded the following optimal parameter values: bond normal contact stiffness of 2.1×10^6 N/m, bond tangential contact stiffness of 2.2×10^6 N/m, and bond radius of 12 mm.

These optimal parameters were subsequently used in simulation tests to determine the firmness of individual soil blocks. The firmness of each block was measured four times to obtain an average value. The results are presented in Table 12. The relative error between the simulated and measured values of the calibrated soil firmness was less than 5%. This close agreement demonstrated that the simulation effectively captured the mechanical properties of actual soil blocks.

Figure 10 depicts the variation of force exerted on the conical steel needle during the actual and simulated firmness measurements. Initially, with no contact, the firmness was 0. As the needle penetrated the soil blocks, the firmness increased until it reached a maximum value at a depth of 30 mm. The measured maximum firmness was 224.1 kPa, while the simulated value was 208.9 kPa. After 3 s, the applied downward force was withdrawn in the actual measurement, leading to a sharp decrease in the measured firmness. This behavior aligned with the changes observed in the bonding forces within the discrete element model of the soil surrounding the conical steel pin (Figure 11). As shown in Figure 11a, the bonding force was negligible before needle insertion into the soil. A significant increase in bonding force was observed during needle penetration (Figure 11b). This force intensified with increasing penetration depth until it began to fracture the bonds. Finally, as shown in Figure 11c, the bonding force and the number of bond breaks in the upper part of the soil blocks reached a peak when the needle reached 30 mm depth. The relative errors between the measured and simulated maximum firmness values for each test group were within 10%. The close similarity between the two curves (Figure 10) further confirmed this agreement. These results validate the accuracy and reliability of the soil blocks modeling approach.

Table 12 Comparison of results for simulation and soil-bin test

Soil block size/mm	Simulation value/kPa	Actual measured value/kPa	Relative error/%
50	194.5	202.9	4.1%
90	202.2	195.4	3.5%
130	200.7	206.5	2.8%

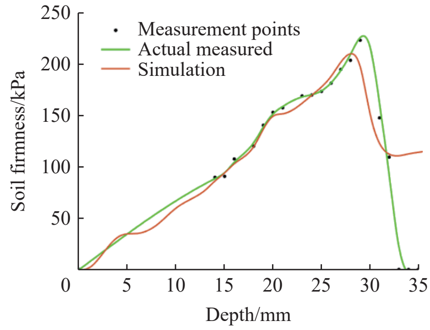

Figure 10 Soil firmness change process

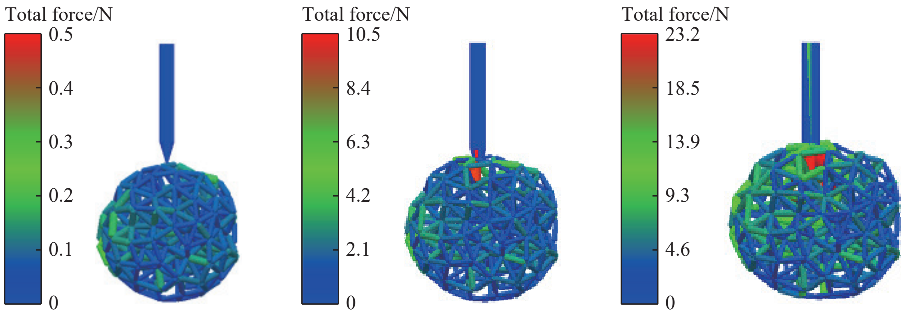

a. Steel needle has not penetrated the soil blocks
b. Steel needle begins to penetrate the soil blocks
c. Steel needle penetrates the soil blocks by 30 mm

Figure 11 Process of force change of soil bonds

4 Verification test of seedbed leveling with seedbed preparation device

4.1 Purpose of the test

To further validate the accuracy of the optimized discrete element model for clay-rich soil blocks, field tests and corresponding simulations were conducted for seedbed soil preparation. Seedbed flatness and firmness were chosen as response variables for comparison and analysis. The relative errors between measured and simulated values were used to assess the accuracy of the discrete element model.

4.2 Test methods and indicators

4.2.1 Field trials on seedbed preparation

Field trials were conducted in the designated testing area at Liuyang Yingchang Agricultural Machinery Specialized Cooperative. To ensure consistent soil conditions across multiple trials, the soil was sequentially treated with stubble removal and rotary tillage before each experiment. Soil parameters were measured, revealing a density of 2680 kg/m^3, a water content of 25.60%, and a firmness of 190.1 kPa at a penetration depth of 50 mm.

A prototype seedbed surface finishing device (Figure 12a) was used for trial production. The operating parameters were as follows: a forming cone roller with a large-end diameter of 450 mm, a pressure roller outer diameter of 130 mm, and a cone inclination angle of 55°. The pressure roller sank 40 mm into the soil during operation, and the device operated at a speed of 290 r/min. The instruments and equipment used primarily included a tractor (DF604-15), the seedbed surface finishing device, a soil firmness JK-750-I tester (Figure 12b), a tape measure, a steel ruler, coordinate paper, a stopwatch, and a marking pen.

a. Test prototype
b. Seedbed surface soil firmness measurement

Figure 12 Field experiment

The field test for compartment flatness involved four repetitions. During each test, the tractor moved in slow first gear (1.62-1.81 km/h) along a straight 20 m path. The middle 10 m of this path, where the implement speed exhibited greater stability, was designated as the test measurement area. Soil firmness on the seedbed surface was measured using the same method employed previously. The recorded numerical results from each test were averaged across the four repetitions to obtain the final results. In addition, the standard deviation was calculated to quantify the variability in the measurements.

4.2.2 Seedbed flatness measuring device and data processing

To precisely assess the flatness of the seedbed surface after pressure roller flattening, a custom-made seedbed surface soil contour measuring instrument was employed. This instrument's design is based on the pin-plate contact contour measurement method[31]. The measurement process is depicted in Figure 13. The seedbed soil contour measuring instrument comprises a base, a stand, a round bar fixing plate, a back plate, a hollow steel round bar, and coordinate paper. The entire device measures 200 mm×1000 mm×800 mm (length×width×height). It utilizes 10 mm×10 mm square coordinate paper for recording measurements. The hollow steel round bar has a diameter of 10 mm and a length of 350 mm. The coordinate paper is affixed to the back plate. Notably, the measuring width of the device exceeds the width of the working seedbed surface, ensuring complete profile measurement.

a. Seedbed surface profile after rotary tillage operation

b. Seedbed surface profile after pressing roller operation

Figure 13 Field experiment of pressing roller operation

Seedbed surface flatness: the local flatness of the seedbed surface was calculated based on the standard deviation of relative elevation of the field surface of the farmland, S_d[32,33], and the measurement was repeated four times to take the average value of S_d and get the overall flatness of the seedbed surface.

$$S_d = \sqrt{\sum_{i=1}^{m} \frac{(H_i - H_0)^2}{(m_0 - 1)}} \tag{4}$$

where, S_d denotes the standard deviation value of relative elevation; H_i represents the relative elevation of the i^{th} sampling point, mm; H_0 represents the relative expected elevation, mm; m_0 denotes the total number of sampling points on the compartment curve.

Relative error: The relative error between the field test results and the simulation test results was calculated. The simulated value was considered the standard value, and the absolute value of the difference between the measured and simulated values was used to determine the relative error.

4.2.3 Simulation test of roller finishing compartments

To ensure the accuracy of the simulation analysis, a three-dimensional model of the pressure roller parts was created in a 1:1 scale and imported into EDEM software after simplification. The model material was set to steel with the same physical parameters as the actual test roller. The pressure roller was configured to rotate clockwise at 290 r/min with a horizontal forward speed of 0.47 m/s, matching the physical test parameters.

Figure 14a depicts the initial state of the simulated soil groove before the pressure roller operation. Once the virtual soil groove was finished by the seedbed surface finishing device in the simulation, the particles within the furrow and ridge sections were isolated and displayed using EDEM's post-processing slicing function. The resulting x-axis direction orthographic view is shown in Figure 14b. To quantify flatness, the contour path was extracted from the binarized front view image and imported into AutoCAD for parameter measurement. Four simulations were conducted to evaluate the flatness of the seedbed surface. The average value of these four parallel tests was recorded as the simulation test result.

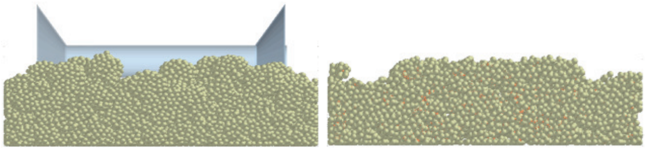

a. Seedbed surface profile after rotary tillage operation

b. Seedbed surface profile after pressing roller operation

Figure 14 Simulation experiment of pressing roller operation

To better illustrate the force distribution and particle crushing within the soil blocks during pressure roller operation, a 200 mm long cross-section of the simulated soil groove was chosen for observation. This section allowed visualization of the crushing process experienced by 130 mm soil particles on the seedbed surface. Figure 15a shows the initial state of the soil blocks before the pressure roller enters the simulated soil groove area. No force is exerted on the soil blocks at this point. As the pressure roller approached the region (Figure 15b), the soil blocks began to experience force. This force was evident by the change in color of the small spherical particles within the block, transitioning from blue to green. With continued forward movement of the pressure roller (Figure 15c), the force on the soil blocks surpassed the bonding force between particles, initiating breakage. This resulted in fragmentation of the soil blocks. Maximum force was applied to the soil blocks when the pressure roller was directly above it (Figure 15d). Consequently, this stage exhibited the most significant fragmentation. As the pressure roller moved further forward (Figure 15e), some of the broken, small spherical particles became unstable due to the force. These particles were then thrown backward and upward. Finally, with the continued forward movement of the pressure roller (Figure 15f), the broken small spherical particles were deposited downward into the region, ultimately contributing to the formation of a relatively flat soil compartment. These broken particles included fragments of various sizes from the original soil blocks.

4.3 Test results and analysis

Figure 13b presents the field test for compartment finishing, while Figure 14 illustrates the corresponding simulation test. Table 13 compares the results of the field test and the simulation test for the seedbed surface finishing device. The results demonstrated that, based on the two contact models (Hertz-Mindlin with JKR and Hertz-Mindlin with Bonding), calibration and optimization of the discrete element model parameters for the clayey soil blocks (using the stacking angle and firmness tests) yielded a simulation that captures the movement patterns of the soil particles with greater accuracy compared to the field test. However, the simulation underestimated the degree of leveling and firmness achieved on the finished seedbed surface. Following parameter calibration and optimization using the stacking angle and firmness tests, the motion patterns of the soil particles in the simulated soil model exhibited closer resemblance to those observed in the field test. The resulting errors in flatness and firmness of the finished seedbed surface were 10.7% and 9.8%, respectively.

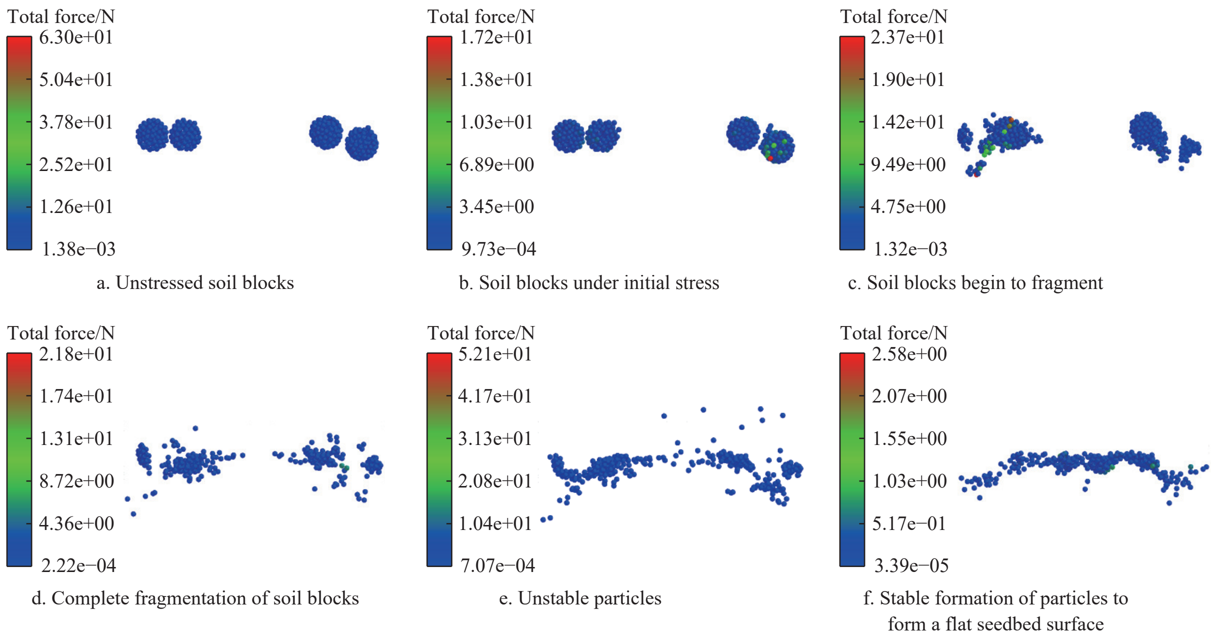

Figure 15 Process of soil blocks fragmentation

Table 13 Comparison of results for simulation and field experiment

Parameter	Measured value	Simulation value	Error /%
Flatness of unleveled seedbed surface/mm	270.7	300.5	11.0
Flatness of seedbed surface after finishing/mm	15.9	14.2	10.7
Firmness of the soil at 50 mm on the surface of the seedbed/kPa	190.1	208.7	9.8

5 Conclusions

This study employed the EDEM discrete element simulation software. Two contact models, Hertz-Mindlin with JKR and Hertz-Mindlin with Bonding, were integrated to simulate and calibrate relevant parameters for clayey soil blocks commonly found in the southern rice-oil multi-maturing zone.

A combination of physical and simulation tests was conducted to optimize the parameters influencing the Hertz-Mindlin with JKR model for interactions between soil aggregates. Design-Expert software was used, targeting the physical stacking angle of clay-rich soil blocks. This optimization yielded a set of optimal parameters: soil-soil static friction coefficient (0.32), soil-soil rolling friction coefficient (0.10), soil-steel static friction coefficient (0.51), and soil JKR surface energy (5.50 J/m^2). The validity of these parameters was confirmed through simulation tests, with a relative error of only 5.1% between the simulated and actual physical stacking angle. Similarly, parameters affecting the Hertz-Mindlin with Bonding model (describing interactions within the clay block) were optimized using the physical firmness of the clay block as the reference value. This resulted in the following optimal parameter combination: bond normal contact stiffness (2.1×10^6 N/m), bond tangential contact stiffness (2.2×10^6 N/m), normal ultimate stress (0.55 MPa), tangential ultimate stress (0.55 MPa), and bond radius (12 mm). Simulation tests again demonstrated high accuracy, with a relative error of less than 5.0% between the simulated and measured firmness. These results effectively validate the reliability of the established simulation model parameters.

The comparison of field and simulation tests for the compartment finishing device revealed that calibration and optimization of the discrete element simulation parameters for clay-rich soil led to improved agreement between the movement patterns of soil particles involved in compartment flattening within the simulated soil model and those observed in the field test. Besides, the discrepancies in both compartment flatness and soil firmness between the field test and simulation test results were found to be within 12.0%.

The study still has limitations that should be acknowledged. First, it did not account for the impact of soil moisture content variations on parameters; future work should calibrate parameters under different moisture conditions. Second, particle shape was simplified using a multi-sphere model, which differs from the irregular morphology of real aggregates. Introducing 3D scanning technology could generate more precise particle geometric models. Subsequent research will investigate the interaction patterns between the rotary-tilled bed surface and the bed-leveling device to significantly improve bed flatness and reduce the impact of uneven beds on planting quality.

Acknowledgements

The authors would like to acknowledge the financial support of the Project Supported by Scientific Research Fund of Hunan Provincial Education Department (23A0193) and Southern Hilly and Mountainous Region Oilseed and Lettuce Combined Seeder (NK202216020101); Hunan Province Oilseed Industry Technology System (HARS-03).

[References]

[1] Shi Y Y, Wang X C, Hu Z C, Gu F W, Wu F, Chen Y Q. Optimization and experiment on key structural parameters of no-tillage planter with straw-smashing and strip-mulching. Int J Agric & Biol Eng, 2021; 14(3): 103–111.

[2] Zeng Z W, Ma X, Cao X L, Li Z H, Wang X C. Critical review of applications of discrete element method in agricultural engineering. Transactions of the CSAM, 2021; 52(4): 1–20. (in Chinese)

[3] Hao Z H, Zheng E L, Li X, Yao H P, Wang X C, Qian S Y, et al. Performance analysis of the soil-contacting parts for no-tillage planters and optimization of blade structure. Transactions of the CSAE, 2023; 39(2): 1–13. (in Chinese)

[4] Zhou J C, Zhang L B, Hu C, Li Z H, Tang J J, Mao K M. Calibration of wet sand and gravel particles based on JKR contact model. Powder Technology, 2022; 397: 117005.

[5] Ma S, Xu L M, Yuan Q C, Niu C, Zeng J, Chen C, et al. Calibration of discrete element simulation parameters of grapevine antifreezing soil and its interaction with soil-cleaning components. Transactions of the CSAM, 2020; 36(1): 40–49. (in Chinese)

[6] Koushkaki H R, Eshkaftaki M M, Nejadian H A. Simulation of draught force during chisel ploughing using discrete element method. Journal of Biosystems Engineering, 2022; 47: 152–166.

[7] Ucgul M, Saunders C, Fielke J M. Discrete element modelling of top soil burial using a full scale mouldboard plough under field conditions. Biosystems Engineering, 2017; 160: 140–153.

[8] Ding Q S, Ren J, Belal E A, Zhao J K, Ge S Y, Li Y. DEM analysis of subsoiling process in wet clayey paddy soil. Transactions of the CSAM, 2017; 48(3): 38–48. (in Chinese)

[9] Xiang W, Wu M L, Lv J N, Quan W, Ma L, Liu J J. Calibration of simulation physical parameters of clay loam based on soil accumulation test. Transactions of the CSAE, 2019; 35(12): 116–123. (in Chinese)

[10] Wang X L, Zhong X K, Geng Y L, Wei Z C, Hu H, Geng D Y, et al. Construction and parameter calibration of the nonlinear elastoplastic discrete element model for no-tillage soil compaction. Transactions of the CSAE, 2021; 37(23): 100–107. (in Chinese)

[11] Dai F, Song X F, Zhao W Y, Zhang F W, Ma H J, Ma M Y. Simulative calibration on contact parameters of discrete elements for covering soil on whole plastic film mulching on double ridges. Transactions of the CSAM, 2019; 50(2): 49–56,77. (in Chinese)

[12] Du J, Heng Y F, Zheng K, Luo C M, Zhu Y H, Zhang J M, et al. Investigation of the burial and mixing performance of a rotary tiller using discrete element method. Soil and Tillage Research, 2022; 220: 105349.

[13] Li M L, Wang L Z, Liao Q X, Liao Y T, Xiao W L, Zhang Q S. Calibration of rototilled soil discrete element parameters after rotary tillage in the preparation process of rapeseed mechanized direct seeding micro-ridge seed bed. Transactions of the CSAE, 2023; 39(20): 10–19. (in Chinese)

[14] Aikins K A, Ucgul M, Barr J B, Jensen T A, Antille D L, Desbiolles J M. Determination of discrete element model parameters for a cohesive soil and validation through narrow point opener performance analysis. Soil and Tillage Research, 2021; 213: 105123.

[15] Wang X Q, Yu G H, Liu N H, Tong J H, Wang Q Y. Calibration of discrete element simulation parameters for greenhouse inferior seedling substrate. Transactions of the CSAM, 2023; 54(12): 359–366. (in Chinese)

[16] Song Z H, Li H, Yan Y F, Tian F Y, Li Y D, Li F D. Calibration method of contact characteristic parameters of soil in mulberry field based on unequal-diameter particles DEM theory. Transactions of the CSAM, 2022; 53(6): 21–33. (in Chinese)

[17] Milkevych V, Munkholm L J, Chen Y, Nyord T. Modelling approach for soil displacement in tillage using discrete element method. Soil and Tillage Research, 2018; 183: 60–71.

[18] Fang H M, Ji C Y, Farman A C, Guo J, Zhang Q Y, Chaudhry A. Analysis of soil dynamic behavior during rotary tillage based on distinct element method. Transactions of the CSAM, 2016; 47(3): 22–28. (in Chinese)

[19] Zhu H B, Wu X, Bai L Z, Qian C, Zhao H R, Li H. Development of the biaxial stubble breaking no-tillage device for rice stubble field based on EDEM-ADAMS simulation. Transactions of the CSAE, 2022; 38(19): 10–22. (in Chinese)

[20] Yang M X. Numerical study on particle crushing of coarse-grained soil based on discrete element method. Master dissertation. Dalian: Dalian University of Technology, 2020; 69p. (in Chinese)

[21] Liu W Z, He J, Li H W, Li X Q, Zheng K, Wei Z C. Calibration of Simulation parameters for potato minituber based on EDEM. Transactions of the CSAM, 2018; 49(5): 125–135, 142. (in Chinese)

[22] Luo S, Yuan Q X, Shaban G, Yang L Y. Parameters calibration of vermicomposting nursery substrate with discrete element method based on JKR contact model. Transactions of the CSAM, 2018; 49(4): 343–350. (in Chinese)

[23] Zhang Z H, Zhao L L, Lai Q H, Tong J. Operation mechanism analysis and experiments of shovel-type rolling soil-engaging components based on DEM-MBD coupling. Transactions of the CSAE, 2022; 38(15): 10–20. (in Chinese)

[24] Sun J B, Liu Q, Yang F Z, Liu Z J, Wang Z. Calibration of discrete element simulation parameters of sloping soil on loess plateau and its interaction with rotary tillage components. Transactions of the CSAM, 2022; 53(1): 63–73. (in Chinese)

[25] Tian X L, Cong X, Qi J T, Guo H, Li M, Fan X H. Parameter Calibration of Discrete Element Model for Corn Straw - Soil Mixture in Black Soil Areas. Transactions of the CSAM, 2021; 52(10): 100–108, 242. (in Chinese)

[26] Xie W, Peng L, Jiang P, Meng D X, Wang X S. Discrete element model building and optimization of double-layer bonding of rape shoots stems at harvest stage. Transactions of the CSAM, 2023; 54(5): 112–120. (in Chinese)

[27] Tu M, Cao T, Wan Z H, Mo H T, Zhang G Z. Calibration and shear experiments of discrete element bonding parameters for water caltrop. Journal of Huazhong Agricultural University, 2023; 42(4): 270–278. (in Chinese)

[28] Jia H L, Deng J Y, Deng Y L, Chen T Y, Wang G, Sun Z J, et al. Contact parameter analysis and calibration in discrete element simulation of rice straw. Int J Agric & Biol Eng, 2021; 14(4): 72–81.

[29] Chen T, Yi S J, Li Y F, Tao G X, Qu S M, Li R. Establishment of discrete element model and parameter calibration of alfalfa stem in budding stage. Transactions of the CSAM, 2023; 54(5): 91–100. (in Chinese)

[30] Wei Z C, Su G L, Li X Q, Wang F M, Sun C Z, Meng P X. Parameter Optimization and test of potato harvester wavy sieve based on EDEM. Transactions of the CSAM, 2020; 51(10): 109–122. (in Chinese)

[31] Wang X Z, Yue B, Gao X J, Zheng Z Q, Zhu R X, Huang Y X. Discrete Element simulations and experiments of disturbance behavior as affected by mounting height of subsoiler's wing. Transactions of the CSAM, 2018; 49(10): 124–136.

[32] Hu L, Du P, Luo X W, Zhou H, Tang L M, Su H Y. Design and experiment on multi-wheel support laser land leveler hanging on tractor. Transactions of the CSAM, 2019; 50(8): 15–21. (in Chinese)

[33] Li Q, Luo X W, Wang M H, Zhao Z X, Xu Y J, Ou Y G, et al. Design of a laser land leveler for paddy field. Transactions of the CSAE, 2007; 23(4): 88–93. (in Chinese)